ADVANCED SENSOR RESEARCH Open Access
www.advsensorres.com

Deep Learning-Assisted Sensitive 3C-SiC Sensor for Long-Term Monitoring of Physical Respiration

Thi Lap Tran, Duy Van Nguyen, Hung Nguyen, Thi Phuoc Van Nguyen, Pingan Song, Ravinesh C Deo, Clint Moloney, Viet Dung Dao, Nam-Trung Nguyen, and Toan Dinh**

In human life, respiration serves as a crucial physiological signal. Continuous real-time respiration monitoring can provide valuable insights for the early detection and management of several respiratory diseases. High-sensitivity, noninvasive, comfortable, and long-term stable respiration devices are highly desirable. In spite of this, existing respiration sensors cannot provide continuous long-term monitoring due to the erosion from moisture, fluctuations in body temperature, and many other environmental factors. This research developed a wearable thermal-based respiration sensor made of cubic silicon carbide (3C-SiC) using a microfabrication process. The results showed that as a result of the Joule heating effect in the robustness 3C-SiC material, the sensor offered high sensitivity with the negative temperature coefficient of resistance of approximately 5,200ppmK^{-1}, an excellent response to respiration and long-term stability monitoring. Furthermore, by incorporating a deep learning model, this fabricated sensor can develop advanced capabilities to distinguish between the four distinct breath patterns: slow, normal, fast, and deep breathing, and provide an impressive classification accuracy rate of ≈ 99.7%. The results of this research represent a significant step in developing wearable respiration sensors for personal healthcare systems.

1. Introduction

Respiration, a fundamental and unceasing biomechanical physiological process, is an indispensable function that persists throughout human life.[1] Physiological respiration, involving breathing rate and depth, exhibits vital signs for clinical monitoring. Sudden changes in breathing patterns can serve as a pathological indicator for conditions such as respiratory distress, asthma, cardiac arrest, sleep apnea, and other respiratory disorders.[1–4] Therefore, continuous monitoring of human breath is paramount for assessing human well-being, diagnosing illnesses, and, in some cases, even saving human lives.

In clinical practice, the respiration rate is measured by clinicians to assess the health status of patients. Manual counting of the expansion/contraction of the chest or abdomen per minute with a timer is standard. This method requires personal focus and can prove challenging when patients are restless, crying, and breathing rapidly or when practitioners must deal with numerous patients simultaneously. Another approach to measuring a patient's exhalation comprises a nasal cannula with pipes inserted into the nostrils.[5,6] However, these devices have drawbacks such as costliness, bulkiness, and uncomfortable breathing in long-term monitoring. Notably, the system used for diagnosing sleep apnea involves polysomnography and comprises lots of cables, very uncomfortable for patients whilst they attempt to sleep. Hence, the development of a novel, affordable and portable option for continuously monitoring of breath patterns that helps to screen sleep related issues, like sleep apnoea in rural and remote location is a pressing need for the present hour.

T. L. Tran, D. Van Nguyen, H. Nguyen, P. Song, T. Dinh
Centre for Future Materials
University of Southern Queensland
37 Sinnathamby Blvd, Springfield, QLD 4300, Australia
E-mail: thilap.tran@unisq.edu.au; Toan.Dinh@unisq.edu.au

The ORCID identification number(s) for the author(s) of this article can be found under https://doi.org/10.1002/adsr.202300159

DOI: 10.1002/adsr.202300159

T. P. Van Nguyen
Thanh Do University
QL32, Kim Chung, Hoai Duc, Ha Noi, Vietnam

R. C Deo
School of Mathematics
Physics and Computing
University of Southern Queensland
Springfield Campus, QLD 4300, Australia

C. Moloney
School of Nursing and Midwifery
University of Southern Queensland
Toowoomba Campus, QLD 4350, Australia

V. D. Dao, N.-T. Nguyen
Griffith University
Gold Coast, Gold Coast Campus, 1 Parklands Dr, Southport, QLD 4215, Australia

Recently, there has been significant progress in respiration monitoring that encompasses both physical[7–9] and gas or chemical breath sensors.[1,10] In terms of physical respiratory monitoring systems, wearable sensors have been developed that detect physical changes during breathing, which include strain and pressure sensors,[11,12] humidity sensors,[8,13,14] thermal sensors,[9,15–19] and acoustic sensors.[20] Among these sensors, the adoption of thermal flow sensors has gained significant interest as they provide directly measurement of respiration flow, are non-invasive, sensitive, real-time monitoring, and cost-effective.[9,16,17,19,21] These devices commonly employ conductive metallic and nanostructure materials, such as metals, graphene, carbon nanotubes (CNTs), silver nanowires, hydrogel, and more, which are typically integrated with flexible and stretchable substrates. For instance, the study of Dinh et al.[17] has reported a low–cost wearable sensor using conductive pencil graphite on a flexible cellular paper substrate for noninvasive real-time respiratory monitoring. However, the use of paper substrate results in low stretchability, which is unsuitable for long-term uses.[22] The study of Jiang et al.[19] introduced the thermal flow breath sensor using metallic layers (Cr/Au) encapsulated in two polyimide films. The sensor can recognize the abnormalities of the breath conditions, such as hypopnea, polypnea, and apnea. However, metals are usually affected by chemical reaction for a long duration. Additionally, Nguyen et al.[21] has demonstrated a thermal flow sensor by aligning CNTs between the electro-spun polyacrylonitrile (PAN) layers, effectively recording normal, deep, and apnea breath in real time.

In spite of significant progress in this rapidly evolving field, the performance of these sensors is not satisfactory for long-term use due to the adverse effects of the ambient environment during its operation. It is noted that human respiration is highly complex, particularly the exhaled gases consisting of more than 800 compounds, including carbon dioxide, nitrogen, oxygen, water vapor,volatile organic components,[11] humidity, and elevated temperature. These can contribute to the degradation in the mechanical and electrical performance of sensing materials in the long-term monitoring process. Furthermore, the biocompatibility performance of nanomaterials such as carbon nanotube still raises concerns in the long-term applications.[23] Therefore, selecting the proper material to overcome those issues is essential.

Silicon carbide (SiC) has been known as an excellent sensing material for sensitive sensors operating in harsh environments thanks to its chemical inertness and stable electrical and mechanical properties.[24–27] For example, SiC has been investigated for application in high temperatures (such as in the combustion engine of an automobile,[25,27] chemically corrosive conditions,[28] and high radiation conditions (such as in space exploration missions)[27,28]). Additionally, compared with silicon (Si), SiC is valued for its biocompatibility and long-lived stability under immersion in simulated biofluid conditions.[27] Among over 200 SiC polytypes, 3C-SiC stands out as its ability to grow on a Si wafer, allowing compatibility with conventional Micro-electromechanical Systems (MEMS) fabrication technologies and reducing the cost.[29] Furthermore, 3C-SiC has emerged as an ideal candidate for developing temperature sensors,[30] and thermal flow sensors[31] because of its high bandgap, low Young's modulus, and fast thermal response.[32,33] These features make 3C-SiC highly suitable for healthcare application. However, to date, there have been no reports demonstrating on the potential of 3C-SiC as a sensing material for respiratory detection. It is worth noting that exhaled breath temperature closely approximates core body temperature, typically around 35°C, as reported in ref. [34], while thermal sensors would require to work at much higher temperatures (e.g., 80°C or above). Therefore, 3C-SiC is an excellent material for making thermal flow sensors for long-term respiratory monitoring.

The monitoring of respiration is essential for diagnosing and monitoring diseases, such as asthma, sleep apnea, and other respiratory-related diseases. However, conventional respiration sensors are typically stand-alone and limited to single-function detection. Recently, there has been growing interest in developing respiration sensors that not only detect respiratory signals but also provide comprehensive data and decision-making support to clinicians through integrated machine learning (ML) algorithms.[4,35,36] These studies purposely aim to provide an automated system to classify breathing patterns, whether normal or abnormal in order to associate these with the presence of disease signals for accurate diagnosis and monitoring. To date, the integration of machine learning with the thermal respiration sensor has not yet been reported. In this study, we employed the one dimensional-convolutional neural network (1D-CNN) algorithm to classify various breath signals from the developed sensor. The advantages of this method include the capability of the algorithm to directly learn from the incoming (real-time) data signals, which would eliminate the need for hand-crafted feature extraction. This method is particularly well-suited for analysing 1D sensor data and remains invariant in interpreting the features of such datasets.[35,37]

The contributions and novelty of this research work are twofold. 1) To develop a sensitive 3C-SiC sensor for physical respiration monitoring and better understand the thermal sensing characteristics capable of accurately continuous monitoring of respiration over extended periods. 2) To test the effectiveness of the 3C-SiC thermal flow sensor integrated with deep learning algorithms and provide automatic classification of respiration signals with high accuracy. In particular, we investigated the sensitivity, linearity, and long-term stability of the developed sensor. Additionally, the 3C-SiC sensor tested real-time breathing by affixing the device to the philtrum of the subject to sense various breath patterns. Furthermore, the 1D-CNN algorithm is employed to classify breath signals derived from sensor data involving slow, normal, fast, and deep breaths with an accuracy of up to 99.7%, beneficial for early warning of respiratory-related diseases and management, such as sleep apnea, asthma. The excellent performance of the 3C-SiC thermal sensor, with its precise various respiratory rates and classification capabilities, provides promising Internet of Medical Things applications in personalized health management.

2. Results and Discussion

2.1. Working Principle and Fabrication 3C-SiC Sensor

Figure 1 illustrates the overall concept and fabrication process of 3C-SiC respiration sensors, and Figure 1a shows more specifically the sensing principle. Basically, the sensing principle behind this sensor based on the hot-film-flow sensing, as reported

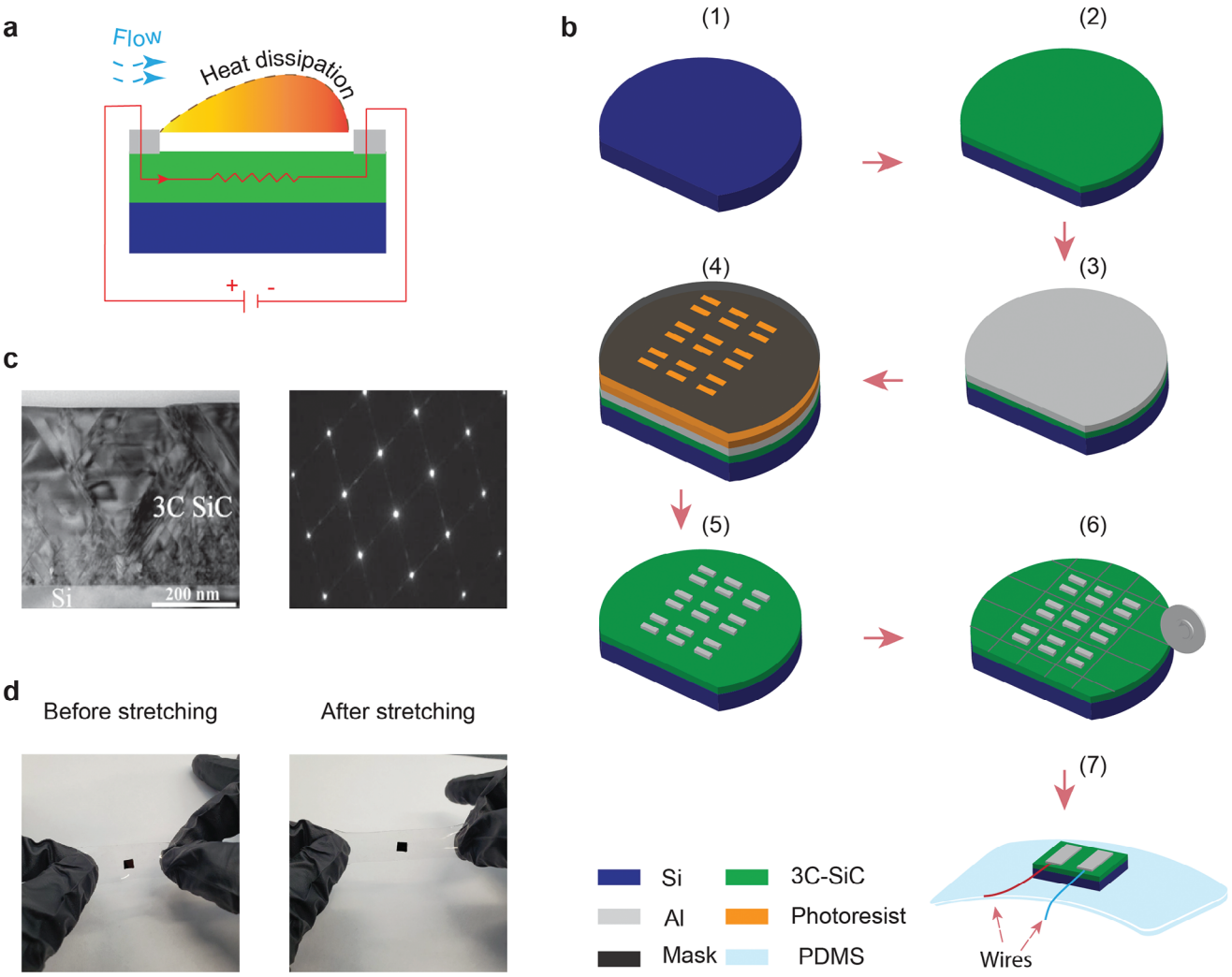

Figure 1. Fabrication and sensing concept of the respiration sensor. a) Working principle of the 3C-SiC thermal flow sensors. b) Fabrication steps of the 3C-SiC respiratory sensor: 1) Preparing Si wafer (100), 2) Grow of 3C-SiC on Si wafer, 3) Deposition of aluminium on the top of 3C-SiC, 4) Photolithography, 5) Etching aluminium, 6) Dicing strips of the 3C-SiC/Si wafer, 7) The sample was attached to stretchable PDMS substrate and making interconnection. c)The crystaline structure of p-3C-SiC grown on (100) Si substrate, TEM image (left), and SAED image (right).[40] d)Optical image of the sample attached to the (polydimethylsiloxane) PDMS substrate.

in ref. [38, 39]. By applying a constant current or voltage to the 3C-SiC thin film, the Joule heating effect causes its temperature to rise. The temperature of the 3C-SiC film subsequently reaches a steady state when supplying Joule heating balances the heat loss to the surroundings. As air passes over the sensor, forced convection causes more heat to be lost to the environment, resulting in a reduction in temperature. As a result, the electrical resistance of the 3C-SiC changes. The airflow rate can be determined by measuring this variation in resistance.

The process of fabricating a wearable 3C-SiC thermal flow sensor consists of seven steps, as outlined in Figure 1b. This process starts with the preparation of the substrate, as indicated in Figure 1b, step 1. A 3C-SiC nanofilm was then grown on a silicon wafer substrate by employing the low-pressure chemical vapor deposition method (LPCVD) (Figure 1b, step 2). The aluminum (Al) was then deposited onto the top of the 3C-SiC nanofilm by sputtering to form electric contact (Figure 1b, step 3). In the next step, a layer of positive photoresist was spin-coated onto the aluminum surface. Here, the shape of the electric contact was patterned by exposing the wafer to ultraviolet light (Figure 1b, step 4). The aluminum electrodes were created by wet etching of aluminum (Figure 1b, step 5). After dicing the strips, the 3C-SiC sample was attached to a stretchable substrate to form the respiration sensor (Figure 1b, step 7).

The crystalline properties of p-3C-SiC on a (100) Si substrate using the LPCVD method are shown in Figure 1c. The left image confirms the transmission electron microscopy (TEM) of the thin film. And the right image shows the selected area electron diffraction (SAED), indicating the single crystalline characteristics of the grown p-3C-SiC on Si substrate. Additionally, Figure 1d indicates the optical images of the device sample formed on a stretchable polydimethylsiloxane (PDMS) substrate before and after stretching. The stretchability of the PDMS substrate is up to approximately 60% strain, meeting the flexibility and

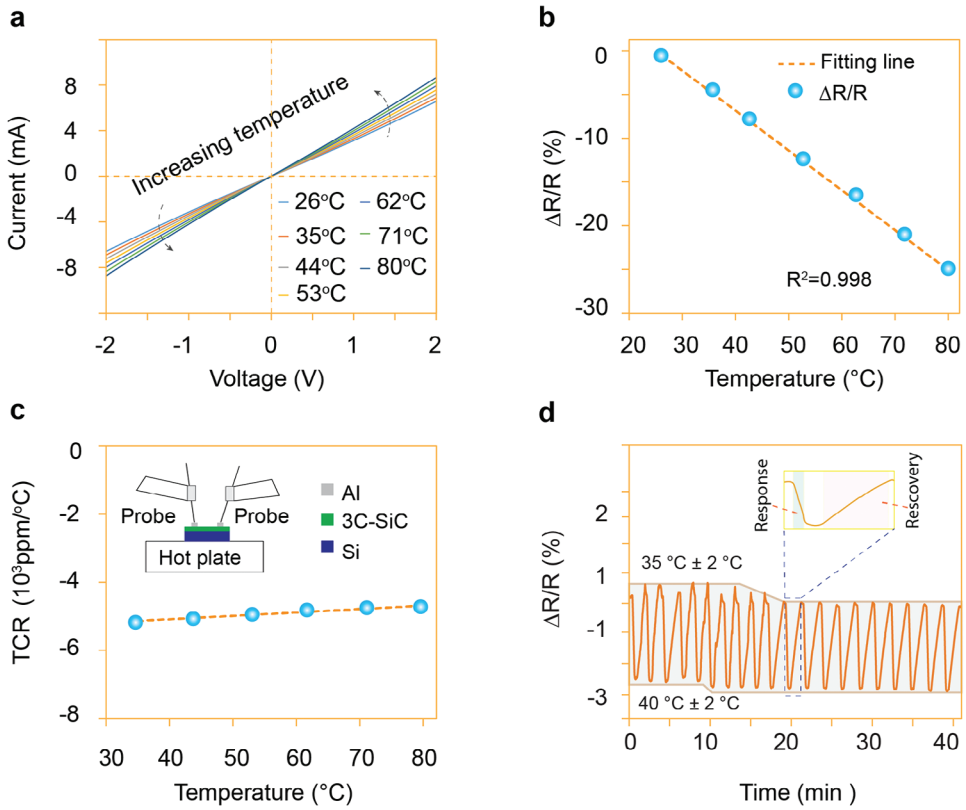

Figure 2. Characterization of the fabricated 3C-SiC sensor. a) *I–V* characteristic of p-3C-SiC measured under different temperatures. b) Relative resistance variation of 3C-SiC versus temperature. c) Temperature coefficient resistance (TCR) of 3C-SiC. Inset: experimental setup to characterize the thermosensitive effect of the thin film. d) Cyclic test of the 3C-SiC based sensor between temperature 35 to 40°C.

stretchability requirements of wearable breath sensors. The PDMS substrate was designed with arrays of tiny holes surrounding the sample for thermal insulation to reduce power consumption.

2.2. Characterization of the 3C-SiC Sensor

As the sensor was specifically fabricated for breath monitoring, which operates at temperatures lower than 80°C, we built an experimental setup to investigate the characteristic of the thermoresistive effect of the 3C-SiC nanofilm under the temperature varying from 26 to 80°C (**Figure** 2c inset). The current- voltage (*I--V)* curves of the fabricated sensor were then measured at different temperature, Figure 2a. The observed linear characteristics indicate an excellent Ohmic contact between 3C-SiC and Al electric contacts across the temperature range. For instance, at a consistent electrical voltage 2 V, the recorded electrical current *I* exhibited a noticeable increase from 6.58 to 8.67 mA with increasing temperature. This is because the increasing temperature leads to a rise in the concentration charge carriers, resulting in a decrease in electrical resistance of the thin film.[26] The correlation between the electrical resistance and temperature can be expressed as follows:[30]

$$R \sim \exp\left(\frac{-E_a}{kT}\right) \quad (1)$$

where E_a denotes the activation energy and and k represents Boltzmann constant.

Figure 2b illustrates the normalized resistance changes derived from the *I–V* data. The relative change in resistance was calculated by $\triangle R/R = (R - R_o)/R$, where R stands for the electrical resistance of the cubic silicon carbide at elevated temperature, R_o denotes the initial resistance. The dependence exhibited a high degree of linearity ($R^2 = 0.9976$), with the resistance decreased by about 25% in response to the temperature rise to 80°C, owning to the negative temperature coefficient of resistance (TCR) of the nanofilm. In general, TCR is commonly defined as the fraction between change in electrical resistance and temperature variation as follows:[39]

$$TCR = \frac{\triangle R}{R}\frac{1}{\triangle T} \quad (2)$$

where $\triangle T$ refers to the variation in temperature. This value is employed to evaluate the sensitivity of thermal flow sensor. A high TCR materials are excellent candidates for a sensitive thermal flow sensors.[24] The high negative TCR value is shown in Figure 2c. As observed from this figure, this value is substantial, approximately of −5, 200 ppmK^{-1}, at around room temperature, and significantly stable in temperature range. This value is comparable to that of other thermal sensing materials in respiration devices. The sensitivity between the developed sensor and

Table 1. Comparing the sensitivity, long-term stability of the developed sensor and previous thermal flow respiration sensors.

Sensor	Materials	Sensitivity (TCR)	Repeatability	Year	Ref.
Thermal flow sensor	Platinum	TCR = 2490ppmK^{-1}	-	2000	[41]
Thermal flow sensor	CNT yarnon paper	TCR= 750ppmK^{-1}	20 cycles	2016	[16]
Thermal flow sensor	Pencil trace on paper	TCR= 2900ppmK^{-1}	one day	2017	[17]
Thermal flow sensor	CNT on paper	TCR= 850ppmK^{-1}	Stability for 30 days	2020	[21]
Thermal flow sensor	Cr/PI	TCR= 3786ppmK^{-1}	–	2020	[9]
Thermal flow sensor	Au/PI	TCR= 3900ppmK^{-1}	–	2020	[19]
Thermal flow sensor	Graphite on paper	TCR= 750ppmK^{-1}	–	2022	[22]
Thermal flow sensor	3C-SiC on polymer substrate	TCR= 5200ppmK^{-1}	Good stability for 90 days		This work

previous ones has been shown in **Table 1**. The TCR varies from −5, 200 ppmK^{-1} to −4, 368 ppmK^{-1} (Figure 2c), which is comparable with other SiC-based thermal sensors.[39] In addition, this value is averagely six times greater than carbon nanotube,[16,21] 1.8 times higher than graphite,[17] and 1.4 times higher than other material (Cr/Au)[9,19] used for thermal flow respiration sensors.

In this study, we have also investigated the repeatability of the 3C-SiC sensor by applying a constant voltage of 2 V to the sensor to conduct a cyclic test within a temperature range of 35 to 40°C. Figure 2d displays the response of the sensor for 20 cycles. The response time and recovery time of the device are approximately 13 s and 72 s, respectively (inset in Figure 2d). The response/recovery time is long because the experiment was conducted at temperature ranging from 35 to 40°C with the increase rate of 30°Cmin^{-1} followed by room temperature cooling condition. The consistency of relative electrical resistance during cyclic tests indicates excellent repeatability of responses from the 3C-SiC thermal sensor. These outstanding characteristics make the fabricated sensor an ideal candidate for continuous long- term respiratory monitoring.

2.3. Respiration Monitoring of 3C-SiC Thermal Flow Sensor

As explained in Section 1, the respiration rate is a vital physiological signal that provides deep insight into the recognition of disease of any patient. In general, the respiration rate refers to the number of breaths one minute or breath per minute (breaths/min). The rate of respiration for healthy adults ranges from 12 to 20 breaths/min, whereas the rate is less than 9 breaths/min, or more than 25 breaths/min is considered irregular. The depth of respiration is the peak-to-peak amplitude measured by respiratory devices. The rate and depth of respiration are sensitive to various factors such as age, gender, weight, and individual health status.[42,43]

In order to evaluate the performance of the developed sensor, the sensor was securely attached to the philtrum of the volunteer, **Figure 3a**. All experiments were conducted under the same surrounding conditions (room temperature of 26°C and a stable humidity approximately of 70%). Thanks to the biocompatibility and stretchability of the respiration device, the volunteer experiences comfort during breathing. According to the sensing principle, when a constant electrical voltage of 5 volts is supplied, the temperature of the device reaches to steady state. When the subject exhales, the temperature of the 3C-SiC thin film decreases, resulting in an increases in the electrical resistance. The change in the temperature of the thin film leads to the change in its resistance. The respiratory rate will be examined by calculating the number peaks of the acquired signals (electrical resistance). Figure 3b shows the change of temperature of the sensor before (left) and after (right) exhalation. The change of $\triangle R/R$ in exhaling and inhaling activities monitored by the sensor for a normal breathing cycle is illustrated in Figure 3c; a peak indicates the moment at which the exhale ended and the inhale started. The number of peaks confirms different breath patterns.

Figure 3d displays the response of the 3C-SiC sensor on normal breathing (0.25 Hz) with the relative change in resistance is approximately 0.46%. This value in slow breath (0.1 Hz) is different because the peak-to-peak values in normal breathing are higher than in slow breathing Figure 3e. However, the period of slow breathing is more significant than that of normal. In contrast, fast breath (0.5 Hz) shows the slightest relative change in resistance of 0.25% (lowest peak-to-peak), as represented in Figure 3f. Regarding deep breathing, the subject exhalation lasted longer than the others, deducing the significant decrease in the temperature of the sensor, leading to the peak-to-peak amplitude of resistance exhibiting a higher of approximately 1.6% (Figure 3g). The breath sensing results demonstrate that the 3C-SiC thermal sensor could detect highly effectively no matter how slow or fast the breath is. Furthermore, these results confirm that the 3C-SiC sensor is more sensitive with respiratory airflow than that of others respiratory devices. For example, the study of Liu et al.[18] developed a hydrogel-based temperature respiratory sensor with relative changes in resistance of about 0.3% for normal breath, while that in our sensor is approximately 0.46%. Nguyen et al.[22] reported a thermal sensor using graphite on paper for human breath monitoring with the relative resistance changes in normal breath is around 0.16%, which is nearly three times less than that of our sensor.

Furthermore, the 3C-SiC respiration sensor underwent testing to assess its performance in detecting sleep apnea. During the test, the volunteer intentionally held their breath three times during normal breathing to simulate sleep apnea episodes, in which their breath is paused for approximately 12 s in each holding time. Figure 3h shows the response of the developed sensor in this experiment. As the sensor operates based on the Joule heating effect, when the volunteer suddenly pauses their breath, the reduction of thermal convection leads to higher temperature around the thin film, causing the decrease in the electrical

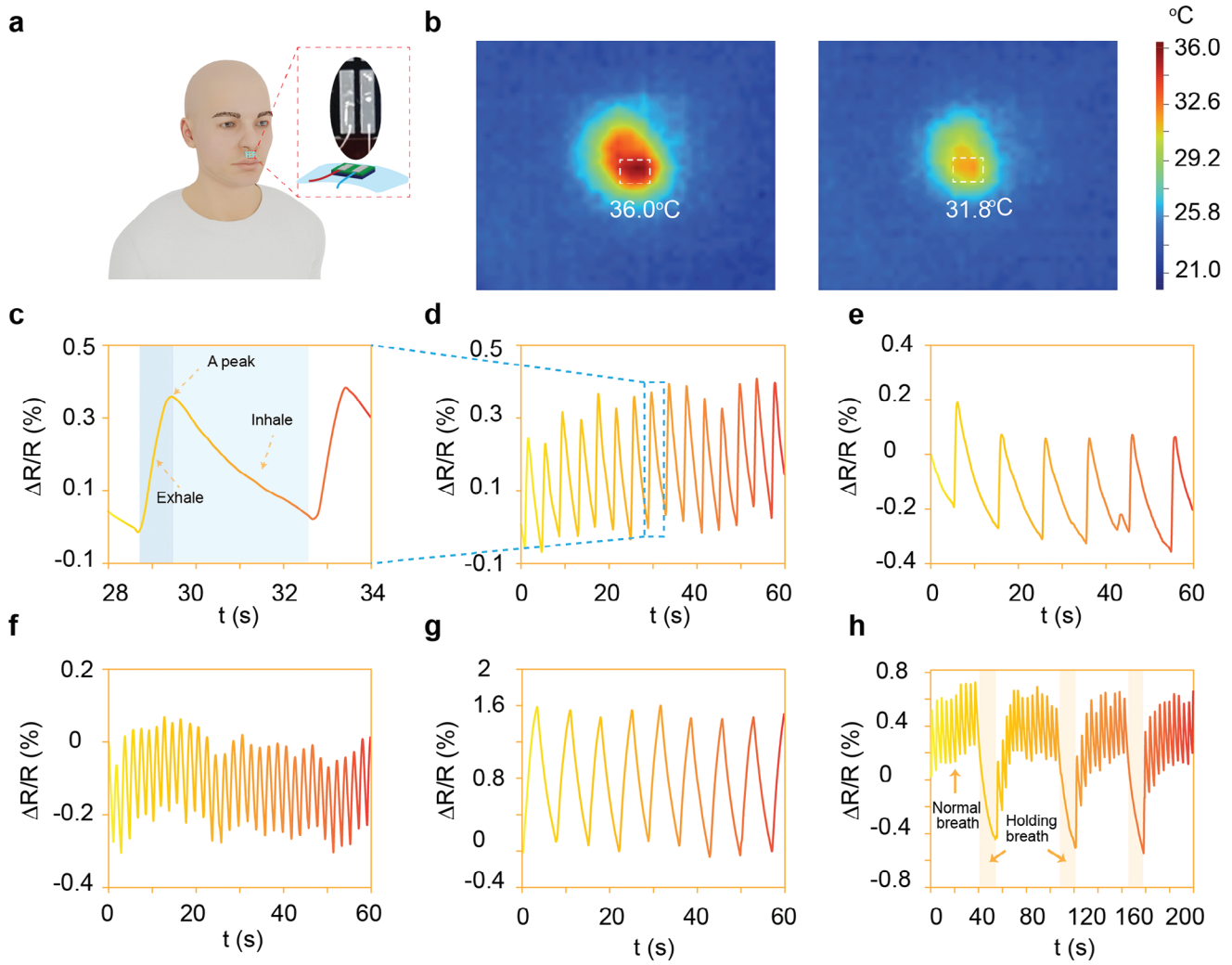

Figure 3. Real-time monitoring of respiration. a) Photograph the fabrication of device was attached to the philtrum of a subject. b) Temperature of the 3C-SiC before and after breathing out. c) A normal breathing cycle. d) Normal breathing (15 bpm). e) Slow breathing (6 bpm). f) Fast breathing (30 bpm). g) Deep breathing (9 bpm). h) Test curve for sleep apnea.

resistance of the film. When the volunteer starts to breathe, the temperature of the sensor decreases, leading to an increase in its resistance. Notably, the key distinguishing between normal breathing and apnea state lies in the continuous waveform versus its discontinuity. By integrating an additional alarm system to alert in the case of threat events, the fabricated sensor is considered a promising option that helps to screen for sleep issues, like sleep apnea.

It is noteworthy that human breath owns more than 800 different chemical compounds, which can interfere with the capability of the 3C-SiC sensor to detect respiration in long-term process. The interfering agents include moisture, nitrogen, oxygen, carbon dioxide, and various residual gases such as ammonia, methane, sulphur dioxide, and volatile organic compounds,[1,11] which may challenge the performance of some sensing materials in continuous long-term monitoring. To assess the long-term durability of the fabricated sensor, we conducted a test by repeating the monitoring respiration experiment over three months with a specific duration each day. **Figure** 4a shows the response of the 3C-SiC respiratory sensor to the normal breath of the volunteer on the first day, one month later, and three months later, respectively. It is noted that the normal breathing patterns were typically consistent in all experiments, confirming the stability of the fabricated sensor over long duration. Furthermore, the response to electrical resistance response of sensor was investigated over three months as shown in Figure 4b. This value was quite consistent each day of testing over three months. The difference ranges from 0,01 to 0.2 Ohm(Ω) by comparing the performance day by day in each month, and about 2 Ω by comparing the performance monthly. The minimal degradation in the electrical resistance values indicates the excellent stability and repeatability of the sensor over the long test. The robustness of the respiration sensor stems from the unique properties of SiC material. SiC with super properties, such as high bandgap (2.38 eV), breakdown voltage (1.2 $MVcm^{-1}$), and melting point(3103K), enhancing both the reliability and stability of SiC devices at elevated temperatures.[26,44] In addition, the high Si-C covalent bond energy (4.6 eV) makes SiC a very inert material that hardly reacts with any other materi-

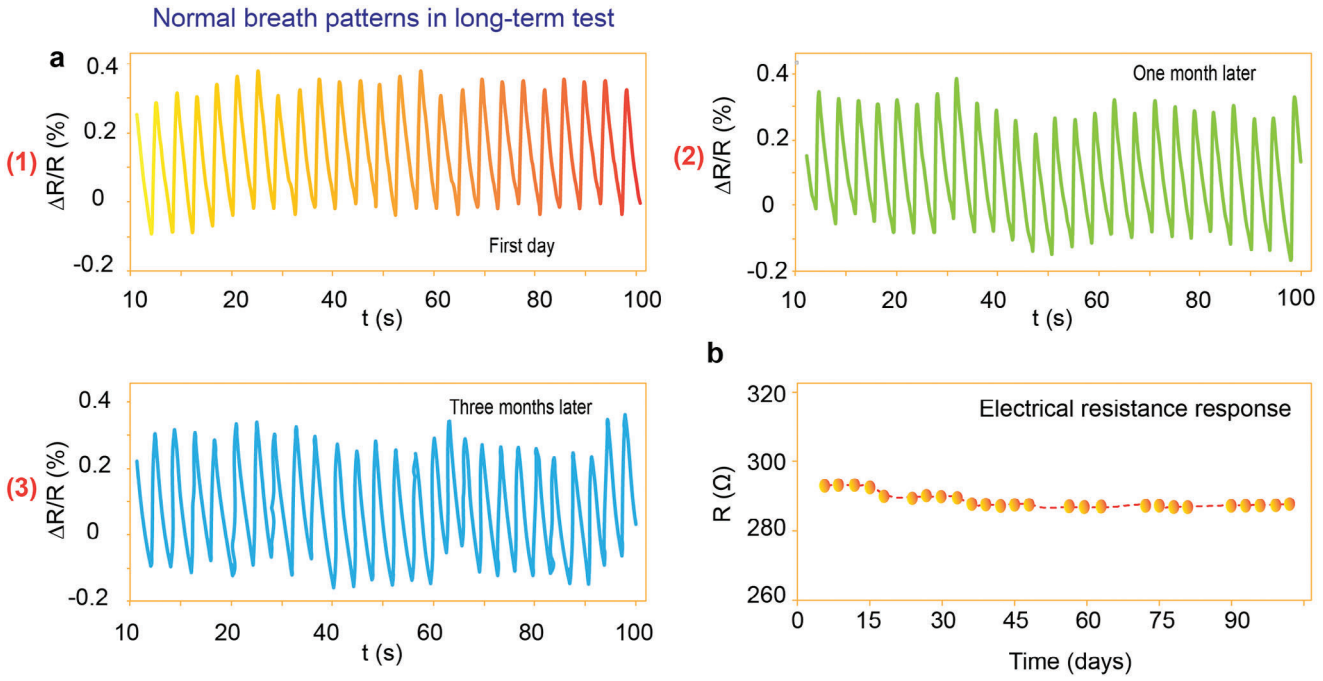

Figure 4. Long-term stability of the 3C-SiC thermal flow sensor. a) Response of the developed sensor to normal breathing at the first day (1), one month later (2), and three months later (3). b) Response of the electrical resistance over three months.

als in room conditions,[24,45,46] allowing it to operate in chemically corrosive conditions.

2.4. Development of Deep Learning Model for the Classification Breath Patterns

Healthcare delivery is changing from its current disease-centric method to a personalized, preventive, predictable mode, focusing on disease prevention, health monitoring, and early issue identification based on analyzing vital signals. In order to improve the precise recognition capability of various respiratory patterns, this study proposes a deep learning model to identify different breath signals from the fabricated sensor that may support early warning, diagnosis of respiratory-related diseases.

In this study, we have adopted the Convolutional Neural Networks (CNN) which is a fundamental algorithm in deep learning classification areas that provides merits relative to the shallow methods. We note that there are several tradition classification models. However, the advantage of the proposed CNN model entails in its advanced capability to directly learn the subtle, yet important features from any real-time data signal without requiring human intervention in the feature extraction stages. Besides, the proposed CNN algorithm can harness significantly large amounts of data to achieve highly promising classification accuracy. Furthermore, the CNN model extends from the traditional artificial neuron networks model by incorporating convolution layers, which help preserve important spatial features of real observations that may be lost or ignored when employing traditional approaches. In respect to prior applications, the CNN model has been extensively used in image classification, including 1D scenarios.[47–50]

It is of particular note that this study has adopted the 1D-CNN model that typically utilizes 1D kernels to interpret 1-D data signal quite effectively by extracting the feature of the fixed-length segment in the entire dataset.[50] Moreover, the 1D-CNN is a viable option to maximize the classification accuracy for many 1D signal applications where the scarce labelled data is concerned.[37,47] A CNN architecture typically consists of three layers: convolution, pooling, and fully connected layers.[48] The convolution layers serve as a pivotal step for feature extraction, as they extract all important features from the diverse input signals. As a result of convolution, feature maps contain a large number of features that are prone to over-fitting. In training, the down-sampling or pooling layer mitigates over-fitting by reducing the spatial dimension of the input signal. The most popular pooling technique is max pooling, which determines the maximum value for each piece of the feature map. Lastly, the feature maps are fed into the fully connected layer, which comprises the number of neurons equal to the number of classes. Each convolution layer typically utilizes a leaky rectifier linear activation function, determining which information should be transmitted to the next neuron. The model is trained with a backpropagation algorithm, and the tuning parameter can be employed to optimize training performance.

The 1D-CNN in this research work consists of three convolutional layers and two fully connected (FC) layers, **Figure 5a**. The fabricated sensor was used to collect four common breathing patterns: slow, normal, fast, and deep. As a result, the respiration signals were then loaded into memory, segmented, and labeled into four categories: slow breathing (S), normal breathing (N), fast breathing (F), and deep breathing (D) (Figure 5a). For class numbers, labels were defined as integers. A 1D-CNN model with multi-class classification was fitted using one-hot

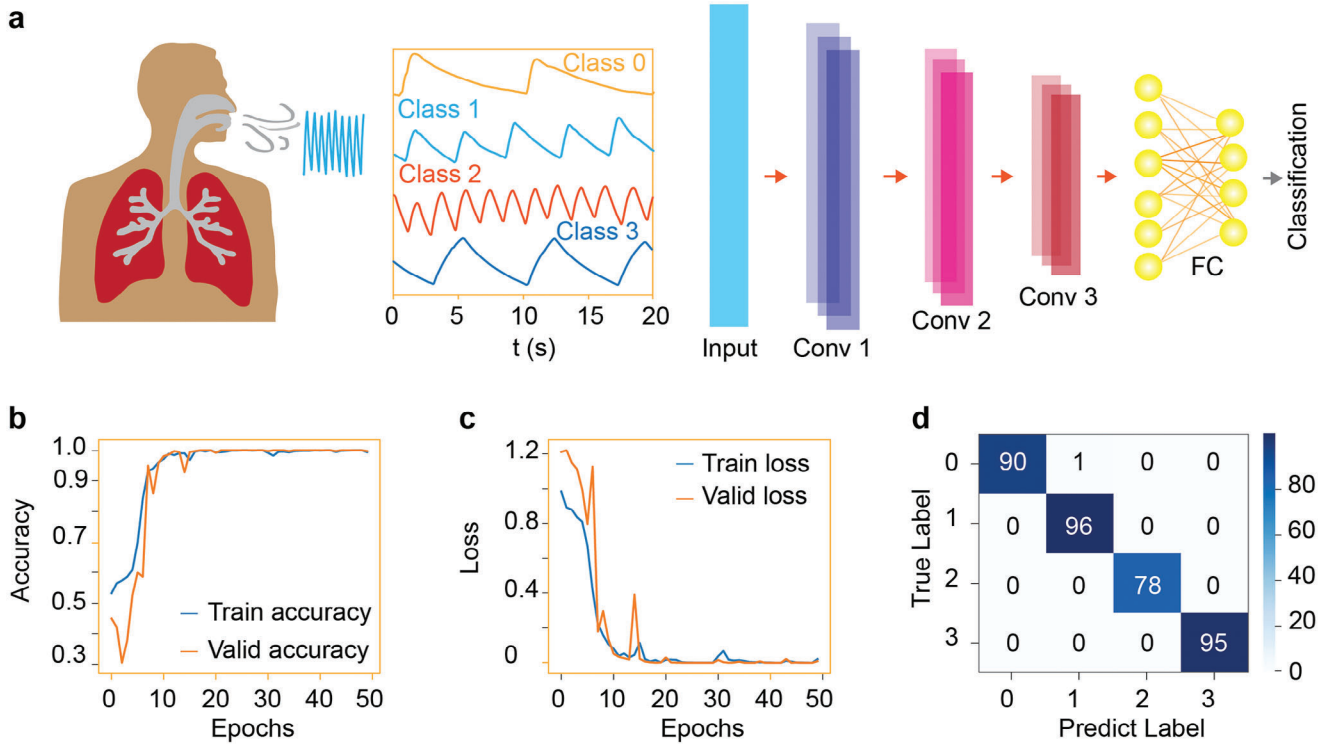

Figure 5. a) The structure of 1D-CNN for classification respiration patterns: Class 0: Slow breathing; Class 1: Normal breathing; Class 2: Fast breathing; Class 3: Deep breathing. b) Training and validation accuracy of respiration data. c) Training and validation loss of the respiration signal. d) Confusion matrix of four types of respiration.

Table 2. Comparing the performance of the proposed 1-D-CNN deep learning model with several previous investigations.

Algorithm	Classification Type	Accuracy, %	Ref.
KNN, DT, RF, BPNN	Normal breath, fast breath, deep breath	Up to 94.0	[36]
DT	Respiration of healthy, asthma, bronchitis, and COPD group	Up to 95.0	[4]
1D-CNN	Four breath patterns: Eupnea, bradypnea, tachypnea, and apnea	Up to 95.8	[51]
1D-CNN	Normal, slow, fast, and deep breath	96.9	[35]
1D-CNN	Normal, slow, fast, and deep breathing	99.7	Our work

encoding for class integers. The effectiveness of the proposed deep learning algorithm was evaluated by learning accuracy, and the loss function. The proposed 1D-CNN model achieved higher classification accuracy and robustness after 50 epochs, as shown in (Figures 5b and 5c). The performance of the proposed system was further evaluated by a confusion matrix, which compared the predicted labels with true labels from the test set. The purpose of this analysis was to determine the ability of the model to differentiate between different breath patterns accurately. The target class (true label) was determined by current output information at the test set, and the output class was determined by the trained 1D-CNN algorithm.

The results of the proposed 1-D-CNN model applied in the classification of different breaths using the real-time signal generated from the 3C-SiC sensor reported an impressive average predictive accuracy of up to 99.7% and the accuracy of an individual class above 98.9%, Figure 5d, which is one of the highest reported accuracy to date, **Table 2**. Furthermore, the proposed 1-D CNN model also outperformed the competing benchmark models based on a Support Vector Machine (SVM) and a Decision Tree (DT) model, which are shown in **Table 3**.

Table 3. Comparing the performance of the proposed 1D-CNN model with a number of traditional machine learning models.

Algorithm	Accuracy	Precision	Recall	F1 score
1D-CNN	0.997	0.997	1.000	0.998
SVM (Extracted features)	0.956	0.958	0.955	0.956
DT (Extracted features)	0.947	0.948	0.948	0.948
DT (Raw data)	0.786	0.783	0.784	0.783
SVM (Raw data)	0.586	0.620	0.577	0.572

3. Conclusion

This research work has demonstrated the successful development and testing of a wearable 3C-SiC thermal flow sensor for real-time respiration monitoring. The developed sensor exhibits impressive sensitivity, boasting a TCR of −5, 200 ppmK^{-1}, and also demonstrates long-term stability, owning to the high performance of the 3C-SiC material under various thermal, humidity, and chemical conditions. Given its accuracy the proposed senor could perhaps excel in terms of its future application to swiftly adapt to various breath rates, making it a powerful tool for detecting abnormal breathing conditions, such as sleep anpea. Furthermore, when integrated with a 1D-CNN model to classify its underlying signals, the present study showed that the deep learning model achieved a remarkable classification accuracy approximately of 99.7% for accurately identifying the diverse breath patterns. In accordance with the findings, the proposed wearable 3C-SiC thermal flow sensor can potentially establish a promising protocol for early picking up any respiratory issues, effectively better self-managing their conditions on day-to-day basis, ultimately alleviating the burden on public healthcare systems. Therefore the present work paves the way for a transition from a disease-centric healthcare model to one that prioritizes personalized care and management in the era of the Internet of Medical Things.

4. Experimental Section

Growth of SiC on Si Substrate: A 300 nm thick 3C-SiC nanofilm was epitaxially grown on a silicon wafer substrate using the LPCVD method at a temperature of 1000°C. Before this process, the p-type Si (100) wafer with a concentration doping level of $5 \times 10^{14} cm^{-3}$ was polished utilizing the standard technique, RCA (Radio Corporation of Americal) to avoid contamination. Here, two precursors, namely silane (SiH_4) and propylene (C_3H_6) were utilized to supply the (Si) and (C). Trimethylaluminum (TMAl) was used as a compound precursor to form a heavily doped p-type 3C-SiC. The carrier concentration of the nanofilm is about $5 \times 10^{18} cm^{-3}$.

Device Fabrication Process: The 3C-SiC respiration sensor was fabricated following the design with the width, length, and thickness of the 3C-SiC layer were 4, 5.5, and 300 nm, respectively. The size of aluminium was 0.6 mm x 2.5 mm. Following the growth process, the conventional photolithography method was employed to pattern the shape of aluminium electrodes using a mask. Here, the spin-coating technique was used to apply a positive photoresist layer onto the aluminium surface at a speed of 3,500 rpm. Before exposing the positive photoresist layer to UV light to create the desired electrode shape, it was heated at a temperature of 110°C for a duration of 100 s. The Al electrodes were created using an Al wet etching technique. The strips were then diced for the proposed devices. Lastly, the 3C-SiC sample was attached to a stretchable Polydimethylsiloxane (PDMS) substrate and interconnections were bonded by a wire-bonding machine (MDB-2575 thin wire Wedge Bonder).

The Fabrication of the PDMS Substrate: To fabricate the PDMS substrate, the curing agent and the elastomer were mixed in a weight-to-weight ratio of 1:10 for 5 min at room temperature. Subsequently, the solution was poured into the mold and stored in the desiccator for approximately 30 min allowing any remaining bubbles to dissipate. The mould was then left at room temperature for 48 h. Lastly, the PDMS slab was diced to make a single substrate.

Characterization and Measurement: The hot chamber was used to evaluate the thermoresistive characterization of the p-3C-SiC nanofilm. The sample was placed on top of the hot plate (Linkam HSF600E-PB4), and probe tips were applied to the aluminium electrodes to connect the nanofilm electrically. The sweep voltage from -2 to 2V is applied, and the *I–V* curve was recorded at temperature ranges from 26 to 80°C with an increment of approximately 9°C.

The resistance data were recorded utilizing a Keithley 2450 Source Meter connected to Kickstart software. The temperature of the sensor was evaluated by capturing images with a thermal imager (Fluke FLK-PTi120 9Hz) by applying the voltage of 5V.

Deep Learning for Breath Patterns Classification: The 1D-CNN architecture was constructed with three convolution layers and two FC layers for data feature extraction and automatic recognition input recorded breath signals. The data used for training and testing contained four different types of breathing, which were acquired from the 3C-SiC sensor.

Four breathing types were continuous collected using the developed sensor using a source meter (Kithey 2450). The raw respiration signal was the analog resistance signal. The signal was loaded into the memory, rearranged, and segmented to be suitable with algorithm using excel and labview 2020 software. This segment data were then label in four different types using python 3.8 with sample size of 166 time-steps. A total of 1800 observations (450 for each breath status) were randomly split into the training and testing set with the rate of 8:2; 80% of the data was used to train the proposed model, and then 20% of the data to evaluate the model. For each training epoch, the accuracy and loss function were assessed to find the optimal classification accuracy and robustness. In this experiments, high breath pattern classification was achieved after 50 training epochs. An analysis of classification accuracy and loss function was then conducted.

Informed Consent Statement: All experiments on monitoring human breath were conducted in accordance with applicable laws and institutional guidelines and approved by the Human Ethics Committee (HREC) of the University of Southern Queensland (H22REA036).

Acknowledgements

The research was funded by the Australian Research Council through grants DE210100852, DP220101252, and DP240102230. The 3C-SiC material was provided by the Queensland Micro-technology Facility, a part of the Griffith Queensland node of the Australian National Collaborative Research Infrastructure Strategy to offer microfabrication and nano services for Australian researchers.

Conflict of Interest

The authors declare no conflict of interest.

Data Availability Statement

The data that support the findings of this study are available from the corresponding author upon reasonable request.

Keywords

convolutional neuron network (CNN), cubic silicon carbide (3C-SiC), long-term monitoring, respiration rate, thermal flow sensor

Received: October 23, 2023
Revised: February 25, 2024
Published online:

[1] Y. Su, G. Chen, C. Chen, Q. Gong, G. Xie, M. Yao, H. Tai, Y. Jiang, J. Chen, *Adv. Mater.* **2021**, *33*, 2101262.
[2] M. Cretikos, J. Chen, K. Hillman, R. Bellomo, S. Finfer, A. Flabouris, MERIT study Investigators, *Resuscitation* **2007**, *73*, 62.

[3] G. Chen, S. Shen, T. Tat, X. Zhao, Y. Zhou, Y. Fang, J. Chen, *View* **2022**, *3*, 20220024.
[4] K. Zhang, Z. Li, J. Zhang, D. Zhao, Y. Pi, Y. Shi, R. Wang, P. Chen, C. Li, G. Chen, I. M. Lei, J. Zhong, *ACS Sens.* **2022**, *7*, 3135.
[5] T. Mauri, C. Turrini, N. Eronia, G. Grasselli, C. A. Volta, G. Bellani, A. Pesenti, *Am J. Respir. Crit. Care Med.* **2017**, *195*, 1207.
[6] V. S. Kumar, C. Krishnamoorthi, *Sens. Actuators A: Phys.* **2021**, *321*, 112582.
[7] T. Dinh, T. Nguyen, H.-P. Phan, N.-T. Nguyen, D. V. Dao, J. Bell, *Biosens. Bioelectron.* **2020**, *166*, 112460.
[8] J. Dai, H. Zhao, X. Lin, S. Liu, Y. Liu, X. Liu, T. Fei, T. Zhang, *ACS Appl. Mater. Interfaces* **2019**, *11*, 6483.
[9] Y. Liu, L. Zhao, R. Avila, C. Yiu, T. Wong, Y. Chan, K. Yao, D. Li, Y. Zhang, W. Li, Z. Xie, X. Yu, *Mater. Today Phys.* **2020**, *13*, 100199.
[10] Y. Su, T. Yang, X. Zhao, Z. Cai, G. Chen, M. Yao, K. Chen, M. Bick, J. Wang, S. Li, G. Xie, H. Tai, X. Du, Y. Jiang, J. Chen, *Nano Energy* **2020**, *74*, 104941.
[11] R. Ghosh, M. S. Song, J. Park, Y. Tchoe, P. Guha, W. Lee, Y. Lim, B. Kim, S.-W. Kim, M. Kim, G.-C. Yi, *Nano Energy* **2021**, *80*, 105537.
[12] Z. Liu, Z. Li, H. Zhai, L. Jin, K. Chen, Y. Yi, Y. Gao, L. Xu, Y. Zheng, S. Yao, Z. Liu, G. Li, Q. Song, P. Yue, S. Xie, Y. Li, Z. Zheng, *Chem. Eng. J.* **2021**, *426*, 130869.
[13] V. Balakrishnan, T. Dinh, A. R. M. Foisal, T. Nguyen, H.-P. Phan, D. V. Dao, N.-T. Nguyen, *IEEE Sens. J.* **2019**, *19*, 11784.
[14] Y. Pang, J. Jian, T. Tu, Z. Yang, J. Ling, Y. Li, X. Wang, Y. Qiao, H. Tian, Y. Yang, T.-L. Ren, *Biosens. Bioelectron.* **2018**, *116*, 123.
[15] N. Nguyen, W. Dötzel, *Sens. and Act* **1997**, *62*, 506.
[16] T. Dinh, H.-P. Phan, T.-K. Nguyen, A. Qamar, A. R. M. Foisal, T. N. Viet, C.-D. Tran, Y. Zhu, N.-T. Nguyen, D. V. Dao, *J. Mater. Chem. C* **2016**, *4*, 10061.
[17] T. Dinh, H.-P. Phan, T.-K. Nguyen, A. Qamar, P. Woodfield, Y. Zhu, N.-T. Nguyen, D. V. Dao, *J. Phys. D: Appl. Phys.* **2017**, *50*, 215401.
[18] J. Liu, H. Wang, T. Liu, Q. Wu, Y. Ding, R. Ou, C. Guo, Z. Liu, Q. Wang, *Adv. Funct. Mater.* **2022**, *32*, 2204686.
[19] T. Jiang, L. Deng, W. Qiu, J. Liang, Y. Wu, Z. Shao, D. Wang, M. Zhang, X. Qian, J. Zhong, X. Wang, L. Lin, *Biosens. Bioelectron.* **2020**, *163*, 112288.
[20] A. Chen, A. J. Halton, R. D. Rhoades, J. C. Booth, X. Shi, X. Bu, N. Wu, J. Chae, *ACS Sens.* **2019**, *4*, 944.
[21] T. Nguyen, T. Dinh, V. T. Dau, C.-D. Tran, H.-P. Phan, T.-K. Nguyen, H. K. Nguyen, F. A. Riduan, P. Guzman, N.-T. Nguyen, D. V. Dao, *IEEE Sens. J.* **2020**, *21*, 7308.
[22] T. Nguyen, N. S. Shagle, H. Vu, H. Nguyen, H.-P. Phan, P. Song, H. Wang, T. D. Quoc, D. T. Nguyen, N.-T. Nguyen, D. V. Dao, T. Dinh, *IEEE Sens. J.* **2022**, *22*, 16804.
[23] S. Smart, A. Cassady, G. Lu, D. Martin, *Carbon* **2006**, *44*, 1034.
[24] V. Balakrishnan, T. Dinh, H.-P. Phan, D. V. Dao, N.-T. Nguyen, *Sens. Actuators A: Phys.* **2018**, *279*, 293.
[25] H.-P. Phan, T. Dinh, T. Kozeki, A. Qamar, T. Namazu, S. Dimitrijev, N.-T. Nguyen, D. V. Dao, *Sci. Rep.* **2016**, *6*, 28499.
[26] T. Dinh, H.-P. Phan, T. Kozeki, A. Qamar, T. Namazu, N.-T. Nguyen, D. V. Dao, *RSC Adv.* **2015**, *5*, 106083.
[27] H.-P. Phan, Y. Zhong, T.-K. Nguyen, Y. Park, T. Dinh, E. Song, R. K. Vadivelu, M. K. Masud, J. Li, M. J. Shiddiky, D. Dao, Y. Yamauchi, J. A. Rogers, N.-T. Nguyen, *ACS Nano* **2019**, *13*, 11572.
[28] Z. Hong, L. Cheng, L. Zhang, Y. Wang, *Int. J. Appl. Ceram. Technol.* **2011**, *8*, 342.
[29] A. R. M. Foisal, T. Dinh, V. T. Nguyen, P. Tanner, H.-P. Phan, T.-K. Nguyen, B. Haylock, E. W. Streed, M. Lobino, D. V. Dao, *IEEE Trans. Electron Devices* **2019**, *66*, 1804.
[30] T. Dinh, D. V. Dao, H.-P. Phan, L. Wang, A. Qamar, N.-T. Nguyen, P. Tanner, M. Rybachuk, *Appl. Phys. Express* **2015**, *8*, 061303.
[31] N.-T. Nguyen, *IEEE Sens. J.* **2005**, *5*, 1224.
[32] H.-P. Phan, H.-H. Cheng, T. Dinh, B. Wood, T.-K. Nguyen, F. Mu, H. Kamble, R. Vadivelu, G. Walker, L. Hold, A. Iacopi, B. Haylock, D. V. Dao, M. Lobino, T. Suga, N.-T. Nguyen, *ACS Appl. Mater. Interfaces* **2017**, *9*, 27365.
[33] H. Nguyen, T. Nguyen, D. V. Nguyen, H.-P. Phan, N.-T. Nguyen, D. Dao, J. Bell, T. Dinh, in: *2022 IEEE Sensors*, IEEE, **2023**, pp.1–4.
[34] T. A. Popov, S. Dunev, T. Z. Kralimarkova, S. Kraeva, L. M. DuBuske, *Respir. Med.* **2007**, *101*, 2044.
[35] N. Bokka, J. Karhade, P. Sahatiya, *J. Mater. Chem. B* **2021**, *9*, 6870.
[36] G. Chen, R. Guan, M. Shi, X. Dai, H. Li, N. Zhou, D. Chen, H. Mao, *Microsyst. Nanoeng.* **2022**, *8*, 44.
[37] S. Kiranyaz, O. Avci, O. Abdeljaber, T. Ince, M. Gabbouj, D. J. Inman, *Mech. Syst. Signal Process.* **2021**, *151*, 107398.
[38] V. Balakrishnan, T. Dinh, T. Nguyen, H.-P. Phan, T.-K. Nguyen, D. V. Dao, N.-T. Nguyen, *Rev. Sci. Instrum.* **2019**, *90*, 1.
[39] T. Dinh, H.-P. Phan, A. Qamar, P. Woodfield, N.-T. Nguyen, D. V. Dao, *J. Microelectromech. Syst.* **2017**, *26*, 966.
[40] A. R. Md Foisal, A. Qamar, H.-P. Phan, T. Dinh, K.-N. Tuan, P. Tanner, E. W. Streed, D. V. Dao, *ACS Appl. Mater. Interfaces* **2017**, *9*, 39921.
[41] S.-T. Hung, S.-C. Wong, W. Fang, *Sens. Actuators A: Phys.* **2000**, *84*, 70.
[42] J. McFadden, R. Price, H. Eastwood, R. Briggs, *Br. Med. J. (Clin. Res. Ed.)* **1982**, *284*, 626.
[43] S. Fleming, M. Thompson, R. Stevens, C. Heneghan, A. Plüddemann, I. Maconochie, L. Tarassenko, D. Mant, *Lancet* **2011**, *377*, 1011.
[44] H.-P. Phan, D. V. Dao, K. Nakamura, S. Dimitrijev, N.-T. Nguyen, *J. Microelectromech. Syst.* **2015**, *24*, 1663.
[45] M. J. Ledoux, S. Hantzer, C. P. Huu, J. Guille, M.-P. Desaneaux, *J. Catal.* **1988**, *114*, 176.
[46] L. Wang, Y. Zhao, Y. Yang, X. Pang, L. Hao, Y. Zhao, J. Liu, *IEEE Trans. Electron Devices* **2022**, *69*, 2009.
[47] T. Ince, S. Kiranyaz, L. Eren, M. Askar, M. Gabbouj, *IEEE Trans. Ind. Electron.* **2016**, *63*, 7067.
[48] O. Faust, Y. Hagiwara, T. J. Hong, O. S. Lih, U. R. Acharya, *Computer Methods and Programs in Biomedicine* **2018**, *161*, 1.
[49] Y. Fang, J. Xu, X. Xiao, Y. Zou, X. Zhao, Y. Zhou, J. Chen, *Adv. Mater.* **2022**, *34*, 2200252.
[50] A. Yildirim, S. Kiranyaz, *IEEE Access* **2020**, *8*, 180534.
[51] S.-H. Kim, G.-T. Han, in *2019 International Conference on Artificial Intelligence in Information and Communication (ICAIIC)*, IEEE, Piscataway, NJ **2019**, pp. 411–414.